Hedgehog signaling regulates epithelial-mesenchymal transition during biliary fibrosis in rodents and humans

Alessia Omenetti,[1] Alessandro Porrello,[2] Youngmi Jung,[1] Liu Yang,[1] Yury Popov,[3,4] Steve S. Choi,[1] Rafal P. Witek,[1] Gianfranco Alpini,[5,6] Juliet Venter,[6] Hendrika M. Vandongen,[1] Wing-Kin Syn,[1] Gianluca Svegliati Baroni,[7] Antonio Benedetti,[7] Detlef Schuppan,[3] and Anna Mae Diehl[1]

[1]Division of Gastroenterology, Department of Medicine, Duke University Medical Center, and [2]Institute for Genome Sciences and Policy, Duke University, Durham, North Carolina, USA. [3]Division of Gastroenterology, Department of Medicine, Beth Israel Deaconess Medical Center, and Harvard Medical School, Boston, Massachusetts, USA. [4]Laboratory of Liver Research, Department of Medicine I, University of Erlangen-Nuremberg, Erlangen, Germany. [5]Central Texas Veterans Health Care System, Temple, Texas, USA. [6]Department of Medicine, Scott & White Hospital and Texas A&M Health Science Center College of Medicine, Temple, Texas, USA. [7]Department of Gastroenterology, Università Politecnica delle Marche, Ancona, Italy.

Epithelial-mesenchymal transitions (EMTs) play an important role in tissue construction during embryogenesis, and evidence suggests that this process may also help to remodel some adult tissues after injury. Activation of the hedgehog (Hh) signaling pathway regulates EMT during development. This pathway is also induced by chronic biliary injury, a condition in which EMT has been suggested to have a role. We evaluated the hypothesis that Hh signaling promotes EMT in adult bile ductular cells (cholangiocytes). In liver sections from patients with chronic biliary injury and in primary cholangiocytes isolated from rats that had undergone bile duct ligation (BDL), an experimental model of biliary fibrosis, EMT was localized to cholangiocytes with Hh pathway activity. Relief of ductal obstruction in BDL rats reduced Hh pathway activity, EMT, and biliary fibrosis. In mouse cholangiocytes, coculture with myofibroblastic hepatic stellate cells, a source of soluble Hh ligands, promoted EMT and cell migration. Addition of Hh-neutralizing antibodies to cocultures blocked these effects. Finally, we found that EMT responses to BDL were enhanced in patched-deficient mice, which display excessive activation of the Hh pathway. Together, these data suggest that activation of Hh signaling promotes EMT and contributes to the evolution of biliary fibrosis during chronic cholestasis.

Introduction

Biliary fibrosis is an outcome of chronic biliary injury in both humans and rodents (1). A number of different cell types are thought to contribute to matrix deposition during chronic cholestasis (1–5), including myofibroblastic hepatic stellate cells (MF-HSCs) (6–8), portal fibroblasts (9–12), and fibrocytes derived from bone marrow (13). Immunostaining of serial liver sections from patients with primary biliary cirrhosis (PBC) recently demonstrated expression of vimentin and other mesenchymal markers in proliferating bile ductules within fibrotic portal tracts, leading the authors to propose that epithelial-mesenchymal transition (EMT) may also play a role in the pathogenesis of biliary fibrosis (14, 15). EMT has been implicated in repair of injury in other adult tissues, such as the kidney (16, 17). It is also an important mechanism for tissue morphogenesis during fetal development (18–20) and tumor metastasis in adults (19–23). Hedgehog (Hh) family ligands regulate EMT during the latter circumstances (22, 24–29).

Hh signaling controls tissue construction and remodeling by regulating the viability and migratory activity of various types of Hh-responsive progenitor cells (30–33). Hh ligands are soluble, lipid-modified morphogens that interact with patched (Ptc), a membrane-spanning receptor on the surface of Hh-responsive cells. This ligand-receptor interaction prevents Ptc from inhibiting its coreceptor, smoothened (Smo). Activated Smo, in turn, initiates a series of intracellular events that culminate in activation and nuclear localization of glioblastoma (Gli) family transcription factors. This promotes transcription of Hh-responsive genes, including several components of the Hh signaling pathway itself, such as Ptc, Gli1, and Gli2. Signaling is turned off when the level of Ptc exceeds that of Hh ligands, permitting "free" Ptc to interact with and inhibit Smo (34). Hh signaling is also abrogated by Hh-interacting protein (Hhip), a factor that binds to Hh ligands and blocks Hh ligand–Ptc interactions (35, 36).

Recently, we demonstrated hepatic accumulation of Hh ligands and activation of the Hh signaling pathway in the livers of bile duct–ligated (BDL) rodents (37, 38) and patients with PBC (39). In the present study we evaluated the hypothesis that the Hh pathway promotes EMT in adult bile ductular cells (i.e., cholangiocytes) by analyzing liver samples from patients and rats with chronic biliary fibrosis and manipulating Hh pathway activity in primary cholangiocytes, cholangiocyte cells lines, and mice subjected to biliary injury. The findings, linking Hh pathway activation with EMT in all systems, strongly support our hypothesis and demonstrate a novel paracrine mechanism by which induction of EMT may contribute to hepatic fibrogenesis during chronic cholestasis.
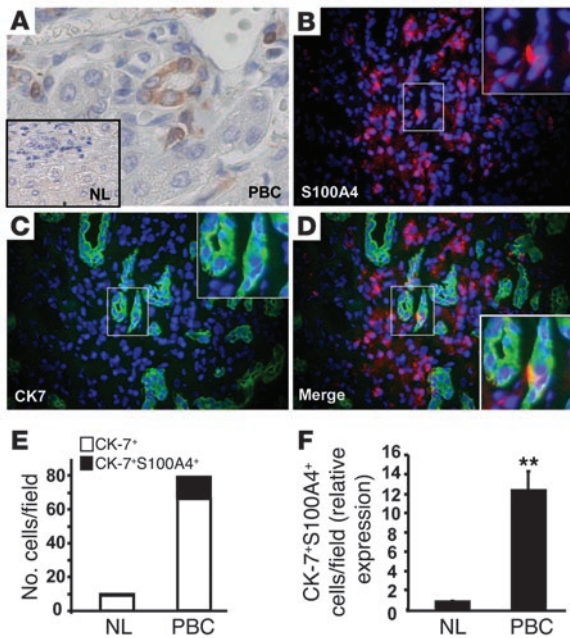
Figure 1
Bile ductular cells express the EMT marker S100A4 in patients with PBC. S100A4 immunostaining in representative sections from control subjects (NL) undergoing resection of metastases from colorectal cancer (**A**, inset) and patients with PBC (**A**). Immunostaining of PBC livers for S100A4 (**B**) and epithelial CK-7 (**C**) demonstrated colocalization of both markers in rare ductular cells (**D**). Ductular appearing cells that expressed CK-7 without or with S100A4 were counted in 20 fields at ×20 magnification in all controls and patients. Data are displayed as mean numbers of CK-7/S100A4 double-positive cells relative to numbers of CK-7 single-positive cells per field (**E**) and mean fold differences in numbers of CK7/S100A4 double-positive cells in PBC patients versus controls (**F**). ****P < 0.005. Original magnification, ×100 (**A**), ×20 (**A**, inset), ×40 (**B**–**D**), ×100 (**D**, inset).

Results

EMT occurs in bile ductular cells of patients with PBC. Liver sections from control subjects without chronic liver disease who were undergoing resection of colorectal metastases and patients with PBC were examined for expression of S100A4 (also called fibroblast-specific protein–1 [FSP-1]), a marker of fibroblastic transformation of epithelial cells (17, 20, 40, 41). Unlike control livers, which demonstrated no S100A4-positive cells (Figure 1A, inset), the livers of PBC patients contained scattered S100A4-positive epithelial-appearing cells within bile ductules, as well as S100A4-positive fibroblastic cells in adjacent stroma (Figure 1A). To verify that this mesenchymal marker was truly expressed by epithelial cells, other PBC liver sections were double immunostained for S100A4 (Figure 1B) and cytokeratin-7 (CK-7), an epithelial marker (42, 43)

(Figure 1C). Colocalization of CK-7 and S100A4 was rarely demonstrated in ductular cells in controls and also occurred in fewer than 20% of CK-7–positive ductular cells in PBC patients (Figure 1, D and E). However, PBC livers had about 12-fold more double-positive ductular cells than controls (Figure 1F), confirming an earlier report (15) that EMT is induced during chronic cholestatic liver disease in humans.

BDL in rats expands populations of cholangiocytes that are undergoing EMT. BDL in rodents is a standard animal model of chronic cholestatic liver damage and biliary fibrosis (4). Roux-en-Y biliary-enteric anastomosis (R-Y) reverses fibrosing cholestatic liver damage in BDL rats, proving that biliary fibrosis is caused by biliary obstruction in this model (37, 44, 45). To clarify the relationship among S100A4, cholestasis, and biliary fibrosis, we isolated total liver RNA from

Figure 2
EMT markers are upregulated in rat cholangiocytes when biliary fibrosis is induced by BDL. (**A**) QRT-PCR analysis of whole liver mRNA expression of *S100a4* in rats with BDL-induced biliary fibrosis (*n* = 8) and BDL rats treated with R-Y to alleviate biliary obstruction and reverse biliary fibrosis (*n* = 5 per each time point). Results were compared with those in sham-operated rats (*n* = 4) and displayed as mean ± SEM. *P < 0.05 versus sham control. (**B**–**E**) QRT-PCR analysis of mRNA from freshly isolated primary cholangiocytes from rats 1 week after BDL. (**B**) *S100a4*; (**C**) *Aqp1*; (**D**) *CK19*; and (**E**) *CK-7*. Results are compared with similar mRNA analysis of freshly isolated cholangiocytes from sham-operated controls. Data are representative of 3 independent experiments and shown as mean ± SEM. *P < 0.05, **P < 0.005 versus sham control.
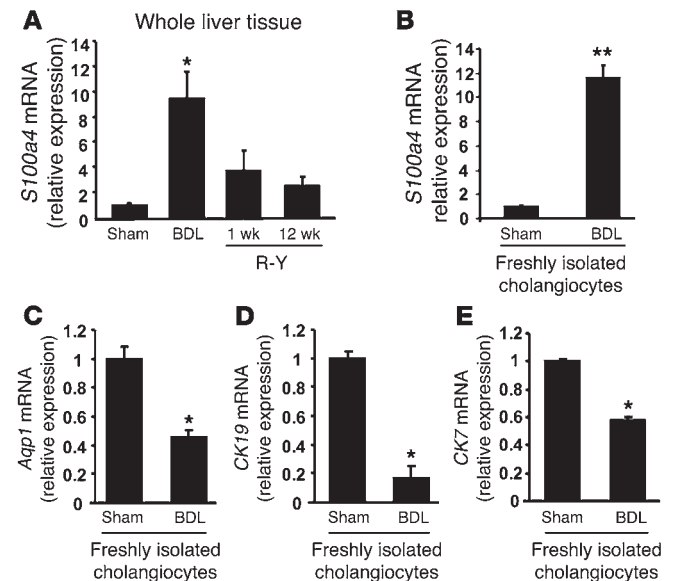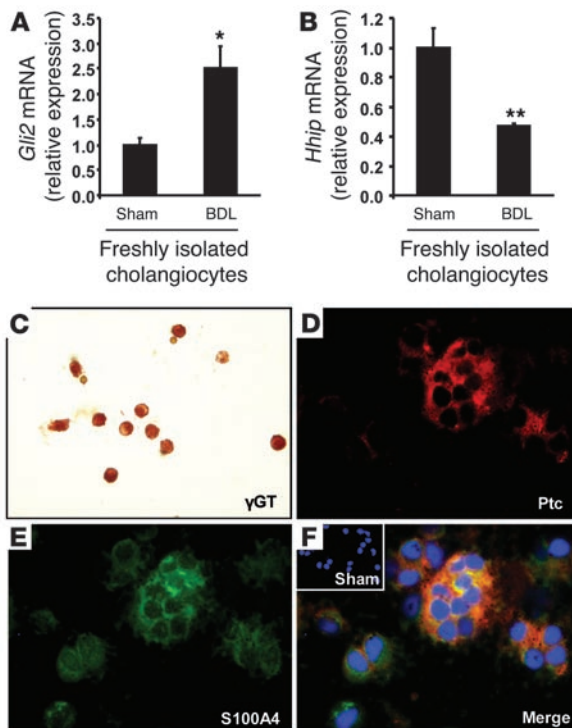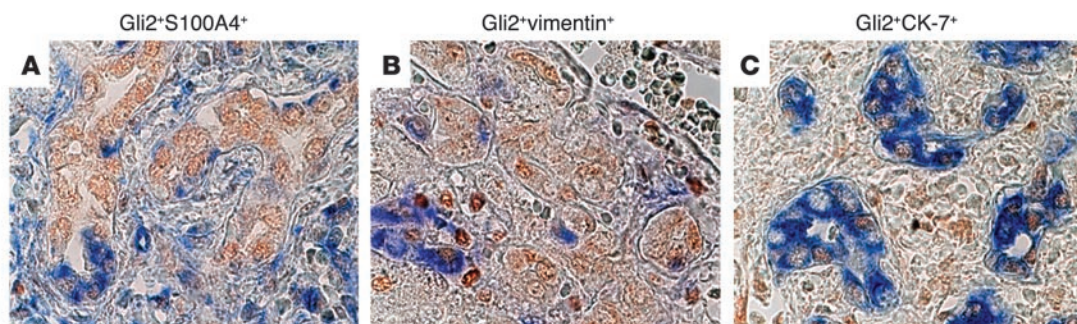
Figure 3
Cholangiocyte populations undergoing EMT during biliary fibrosis in rats are Hh responsive. (**A** and **B**) QRT-PCR analysis of the Hh-inducible transcription factor *Gli2* (**A**) and Hh ligand inhibitor *Hhip* (**B**) in primary cholangiocytes isolated from 1-week BDL rats or sham-operated controls (*n* = 3). Data are shown as mean ± SEM. *$P < 0.05$, **$P < 0.005$ versus sham-operated controls. Immunohistochemistry showing γ glutamyl transpeptidase (γGT) staining in primary cholangiocytes from BDL rats (**C**) and expression of Ptc (**D**) and S100A4 (**E**) in the same preparation. Merged images of S100A4/Ptc in cholangiocytes from BDL rats (**F**) and sham-operated controls (**F**, inset). Original magnification, ×20 (**C**), ×100 (**D–F**), ×20 (**F**, inset).

assessed mRNA expression of aquaporin-1 (*Aqp1*), a ubiquitous cholangiocyte marker (47); *CK19*, a marker of mature cholangiocytes (42); and *CK7*, a marker of immature cholangiocytes (42). Compared with cholangiocytes isolated from sham-operated rats, cholangiocytes from BDL rats expressed significantly less *Aqp1*, *CK19*, and *CK7* (Figure 2, C–E), providing further evidence that chronic cholestasis stimulated cholangiocytes to undergo EMT.

Hh pathway activity increases in cholangiocytes after BDL in rats. The Hh pathway regulates EMT (22, 28, 48), and EMT occurs in human and rodent cholangiocytes during chronic cholestasis (14, 15, 49). Previously, we showed that expression of Hh ligands and Hh target genes is increased in the livers of rodents that have undergone BDL (37, 38) and gradually decline to basal levels when biliary obstruction is relieved by R-Y (37). To examine the effect of BDL on Hh signaling in cholangiocytes, we compared expression of an Hh-inducible gene, *Gli2*, and *Hhip*, an Hh ligand inhibitor, in cholangiocytes from sham-operated controls and BDL rats. BDL upregulated expression of *Gli2* (Figure 3A), while suppressing expression of *Hhip* (Figure 3B). To prove that EMT occurred in cholangiocytes that were Hh responsive, cholangiocytes were isolated from BDL rats and examined by immunocytochemistry. Analysis of γ glutamyl transpeptidase (γGT), an established cholangiocyte marker, demonstrated that these cholangiocyte isolates were very homogeneous, eliminating concerns that the data might have been biased by inclusion of contaminating cell types (Figure 3C). Moreover, the vast majority of these cells expressed Ptc (the Hh receptor that is also an Hh target gene), and most of these were also S100A4 positive (Figure 3, D and F). In contrast, cholangiocytes from sham-operated controls expressed neither Ptc nor S100A4 (Figure 3F, inset). Together with the data displayed

rats 4 weeks after BDL, as well 1 and 12 weeks after R-Y had been performed to relieve biliary obstruction, reverse biliary fibrosis, and restore normal hepatic architecture (37). *S100a4* mRNA expression was examined by quantitative RT-PCR (QRT-PCR) analysis, and results were compared with those in sham-operated controls. BDL caused about a 10-fold increase in whole liver expression of *S100a4*, and biliary decompression reversed this (Figure 2A). Comparison of *S100a4* expression in primary cholangiocytes isolated from sham-operated and BDL rats demonstrated that cholangiocytes from BDL rats expressed 10-fold-higher levels of *S100a4* mRNA than cholangiocytes from sham-operated controls (Figure 2B). Thus, during biliary fibrosis, expression of *S100a4*, a mesenchymal marker of EMT, is upregulated in cholangiocytes.

During EMT, epithelial cells that have induced mesenchymal markers downregulate epithelial markers (16, 20, 46). To determine whether this occurred in cholangiocytes after BDL, we

Figure 4
Cholangiocyte populations undergoing EMT during biliary fibrosis in humans are Hh responsive. Gli2 (brown) localized in nuclei of ductular cells expressing S100A4 (**A**), vimentin (**B**), and CK-7 (**C**) in representative liver sections from PBC patients. Positivity for S100A4, vimentin, or CK-7 is shown as blue cytoplasmic staining. Original magnification, ×100 (**A–C**).
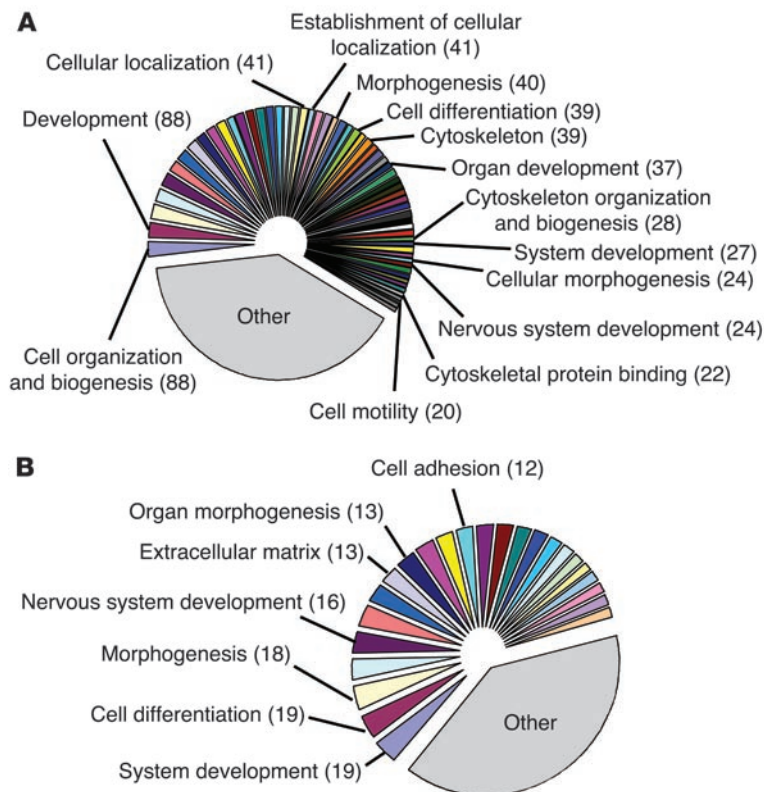
Figure 5
Soluble factors released by myofibroblasts change the gene expression profile of cocultured cholangiocytes. (**A** and **B**) GO analysis of microarray data from cholangiocytes cocultured with MF-HSCs, compared with cholangiocyte monocultures. Each gene probe having an expression ratio above 1.500 and below 0.666 was then assigned to its corresponding GO families. GO sets were therefore ranked based on the total number of genes belonging to them. GO families associated with more than 10% of selected genes were discarded, in order to increase the specificity of the GO analysis. This subpopulation of GO sets was further split into 2 groups, one accounting for at least 60% of this subpopulation, and the other one accounting for the remaining percentage (<40%). A pie chart was then generated using individual names for the first group of GO families, while GO sets belonging to the second group were collectively designated as "other." (**A**) Upregulated GO gene sets. (**B**) Downregulated GO gene sets. Numbers in parenthesis represent altered genes belonging to that specific family. Original pie charts and legends are provided as Supplemental Figures 1 and 2. Complete lists of GO families and EASE scores are reported in Tables 1 and 2 and Supplemental Table 2.

in Figure 2, these results suggest that during chronic cholestasis, cholangiocytes become more Hh responsive and undergo EMT.

Bile ductular cells undergoing EMT in patients with PBC are Hh responsive. To further clarify the relationship between Hh pathway activation and EMT, immunohistochemistry was performed in liver samples from PBC patients. The Hh-inducible transcription factor Gli2 localized in the nuclei of ductular cells that coexpressed various mesenchymal markers (20, 46), such as S100A4 (Figure 4A) and vimentin (Figure 4B), and epithelial cytokeratins (42), such as CK-7 (Figure 4C). Thus, during chronic cholestasis, EMT occurs in ductular cells that are Hh responsive in humans, as it does in rats (Figures 2 and 3).

Soluble factors released by myofibroblasts induce EMT in cholangiocytes. To more directly evaluate the role of Hh signaling in cholangiocyte EMT, we cocultured a cholangiocyte cell line with clonally derived MF-HSCs. During chronic cholestasis, bile ductular cells and myofibroblastic cells typically accumulate near each other within fibrous septae (4), and in earlier studies, we had demonstrated that MF-HSCs are a rich source of Hh ligands (50, 51). In the present study, the cholangiocytes were cultured in Transwells in the absence or presence of the liver myofibroblasts, RNA was isolated, and microarray analysis was done to determine how myofibroblast-derived factors altered cholangiocyte gene expression. Coculture with MF-HSCs significantly upregulated 965 genes and downregulated 235 genes by at least 1.5-fold in cholangiocytes (Supplemental Table 1; supplemental material available online with this article; doi:10.1172/JCI35875DS1). Gene ontology (GO) analysis revealed that most of the differentially expressed genes regulated various processes that were involved in tissue morphogenesis (Figure 5, A and B, Tables 1 and 2, Supplemental Table 2, and Supplemental Figures 1 and 2). Multiple genes that promote

EMT were upregulated, including insulin-like growth factor I receptor 1 (*Igf1r*) (22, 46), high-mobility group AT-hook 2 (*Hmga2*) (52), SMAD-specific E3 ubiquitin protein ligase 1 (*Smurf1*) (46), and cysteine-rich transmembrane BMP regulator 1 (chordin-like) (*Crim1*) (53), while other genes that inhibit EMT, such as bone morphogenetic protein 7 (*Bmp7*) (20, 46), were downregulated (Figure 6A). Various mesenchymal markers (20, 46), such as fibronectin, laminin β3, filamin, and N-cadherin, were concomitantly increased, while epithelial markers (20, 46), such as desmoplakin, declined (Figure 6B). These microarray results were validated by subsequent QRT-PCR analysis (Figure 6C), verifying that soluble factors released from the MF-HSCs induced gene expression changes typical of EMT in cholangiocytes. Although coculture of cholangiocytes with MF-HSCs increased expression of *S100a4* by only 33% in the microarrays (Figure 6B and Supplemental Table 1), QRT-PCR analysis demonstrated that this mesenchymal marker was increased 1.7-fold in cocultured versus monocultured cholangiocytes (Figure 6C), confirming our other evidence that *S100a4* induction correlates with EMT in cholangiocytes.

To determine whether the MF-HSC–derived factors in the coculture system were merely enhancing changes in EMT-related genes that might occur "spontaneously" during culture, cholangiocyte expression of *S100a4* (a marker of EMT) and *Bmp7* (an inhibitor of EMT) were assessed after 3 or 6 days of mono- or coculture. Results were compared with gene expression in freshly plated cholangiocyte monocultures (Figure 7, A and B). When placed in monoculture, cholangiocytes gradually reduced their expression of *S100a4* but increased their expression of *Bmp7*, suggesting a spontaneous tendency to suppress EMT and acquire a more epithelial phenotype during culture. In contrast, cocultured cholangiocytes significantly upregulated *S100a4* and exhibited less induction of

Table 1
Upregulated GO gene sets in cocultured cholangiocytes

GO family[A]	Gene count[B]	Percentage[C]	EASE score
Cell organization and biogenesis	88	9.95%	7.92000×10^{-7}
Development	88	9.95%	7.77000×10^{-5}
Biopolymer modification	86	9.73%	5.94000×10^{-9}
Protein modification	82	9.28%	2.39000×10^{-8}
Transferase activity	73	8.26%	2.03398×10^{-3}
Protein complex	72	8.14%	1.74018×10^{-2}
Purine nucleotide binding	70	7.92%	2.46000×10^{-4}
Adenyl nucleotide binding	59	6.67%	3.15000×10^{-4}
ATP binding	58	6.56%	2.39000×10^{-4}
Non-membrane-bound organelle	55	6.22%	6.66968×10^{-3}
Intracellular non-membrane-bound organelle	55	6.22%	6.66968×10^{-3}
Transferase activity, transferring phosphorus-containing groups	52	5.88%	1.53000×10^{-4}
Kinase activity	50	5.66%	1.94000×10^{-5}
Transcription regulator activity	49	5.54%	4.94198×10^{-3}
Organelle organization and biogenesis	47	5.32%	5.51000×10^{-4}
Intracellular signaling cascade	45	5.09%	1.05950×10^{-3}
Response to stress	44	4.98%	3.15927×10^{-2}
Phosphorus metabolism	42	4.75%	6.09000×10^{-4}
Phosphate metabolism	42	4.75%	6.09000×10^{-4}
Establishment of cellular localization	41	4.64%	1.24000×10^{-5}
Cellular localization	41	4.64%	1.52000×10^{-5}
Intracellular transport	40	4.52%	2.50000×10^{-5}
Phosphotransferase activity, alcohol group as acceptor	40	4.52%	5.50000×10^{-5}
Protein localization	40	4.52%	5.51000×10^{-5}
Morphogenesis	40	4.52%	1.09671×10^{-2}
Establishment of protein localization	39	4.41%	4.70000×10^{-5}
Negative regulation of biological process	39	4.41%	4.83000×10^{-4}
Cytoskeleton	39	4.41%	1.27384×10^{-3}
Cell differentiation	39	4.41%	1.17331×10^{-2}
Protein transport	38	4.30%	4.71000×10^{-5}
Protein kinase activity	37	4.19%	2.62000×10^{-5}
Negative regulation of cellular process	37	4.19%	4.09000×10^{-4}
Phosphorylation	37	4.19%	5.42000×10^{-4}
Organ development	37	4.19%	5.72216×10^{-2}
Ubiquitin cycle	36	4.07%	1.44000×10^{-7}

[A]Top 35 GO sets that were upregulated in cocultured cholangiocytes compared with monocultures. [B]Absolute number of genes altered. [C]Percentage of genes altered within the GO family. The complete list is provided in Supplemental Table 2.

Bmp7 than monocultured cells. These findings demonstrate that the soluble MF-HSC–derived factors actually opposed "spontaneous" cholangiocyte tendencies to become more epithelial in culture by driving the cells to undergo EMT.

Increased cell motility/migration is one of the key phenotypic alterations that accompanies EMT (19, 20, 22, 46). Therefore, we compared cell migration in mono- and cocultured cholangiocytes to verify that the changes in cholangiocyte gene expression that occurred during coculture with MF-HSCs were associated with the acquisition of an EMT phenotype. Cholangiocytes were cultured in the absence or presence of Transwell filter inserts containing MF-HSCs for 6 days; thereafter, the inserts were removed, and the cholangiocyte monolayers were scratched (wounded). Monolayers were photographed immediately (time 0, Figure 8, A and C) and 18 hours later (Figure 8, B and D). Cholangiocyte migration was assessed by measuring the dimensions of the wound dividing the 2 sides of the monolayer (Figure 8G) and by counting the numbers of cells that had migrated into the wound (Figure 8H). Little, if any, cell migration was observed in monocultured cholangiocytes by either assay, whereas the cholangiocytes that had been cocultured with MF-HSCs migrated into the wound, significantly shrinking the gap that had been created between the 2 sides of the monolayer. These findings demonstrate that coculture with MF-HSCs increased cholangiocyte motility/migration and support the concept that factors released from the MF-HSCs induced EMT in the cocultured cholangiocytes.

Neutralization of myofibroblast-derived Hh ligands inhibits EMT in cocultured cholangiocytes. To determine whether soluble, myofibroblast-derived Hh ligands contributed to the induction of EMT in cholangiocytes, wounding studies were repeated in cholangiocyte cocultures and either control IgG (Figure 8D) or Hh-neutralizing antibody (Figure 8F) were added at the time of "wounding" on day 6. Eighteen hours later, cell migration was analyzed (Figure 8, G and H). Treatment with control IgG did not inhibit cholangiocyte migration. However, treatment with Hh-neutralizing antibody reduced migration by about 60% ($P < 0.005$ versus control or IgG-treated cocultures), demonstrating that MF-derived Hh ligands promoted cholangiocyte migration. To determine the effects of MF-derived Hh ligands on cholangiocyte expression of EMT-related genes, monocultures of cholangiocytes were treated with MF-HSC–conditioned medium that contained Hh-neutralizing antibodies or control IgG. (It was not possible to use Hh-neutralizing antibody in the 6-day coculture system, as the Hh-neutralizing antibodies, but not control IgG, killed the MF-HSCs, consistent with our earlier evidence that Hh ligands function as autocrine viability factors for MF-HSCs; refs. 50, 51.) Addition of Hh-neutralizing antibodies to MF-HSC–conditioned medium significantly attenuated the effects of MF-HSCs on cholangiocyte expression of multiple EMT-related genes (Figure 9, A and B). These findings support the concept that paracrine activation of the Hh pathway induces EMT in cultured cholangiocytes.

Ptc-deficient mice with increased Hh activity exhibit increased EMT after BDL. To determine whether Hh pathway activation plays a similar role in cholestasis-related EMT, we subjected mice with haploinsufficiency of the Hh pathway inhibitor Ptc and their WT littermates to BDL and examined EMT markers 1 week later. Ptc-deficient mice (Ptc mice) are unable to repress Hh signaling fully and are susceptible to diseases that result from excessive Hh pathway

Table 2
Downregulated GO gene sets in cocultured cholangiocytes

GO family[A]	Gene count[B]	Percentage[C]	EASE score
System development	19	9.50%	2.50000×10^{-6}
Cell differentiation	19	9.50%	1.44667×10^{-3}
Morphogenesis	18	9.00%	4.64778×10^{-3}
Transcription regulator activity	17	8.50%	4.19175×10^{-2}
Nervous system development	16	8.00%	5.58000×10^{-5}
Cellular biosynthesis	16	8.00%	5.09959×10^{-2}
Extracellular matrix (sensu Metazoa)	13	6.50%	4.60000×10^{-6}
Extracellular matrix	13	6.50%	5.35000×10^{-6}
Organ morphogenesis	13	6.50%	1.95787×10^{-3}
Calcium ion binding	13	6.50%	4.50772×10^{-2}
Transcription factor activity	13	6.50%	6.77121×10^{-2}
Cell adhesion	12	6.00%	1.59211×10^{-2}
Peptidase activity	12	6.00%	4.76787×10^{-2}
Positive regulation of biological process	12	6.00%	5.16325×10^{-2}
Positive regulation of cellular process	11	5.50%	3.99083×10^{-2}
Macromolecule biosynthesis	11	5.50%	8.17202×10^{-2}
Neuron differentiation	9	4.50%	1.76576×10^{-3}
Neurogenesis	9	4.50%	3.57581×10^{-3}
Angiogenesis	8	4.00%	8.75000×10^{-5}
Blood vessel morphogenesis	8	4.00%	2.77000×10^{-4}
Blood vessel development	8	4.00%	6.58000×10^{-4}
Vasculature development	8	4.00%	7.36000×10^{-4}
Enzyme-linked receptor protein signaling pathway	8	4.00%	5.31353×10^{-3}
Sequence-specific DNA binding	8	4.00%	3.44461×10^{-2}

[A]GO sets that were downregulated in cocultured cholangiocytes compared with monocultures.
[B]Absolute number of genes altered. [C]Percentage of genes altered within the GO family.

activation (54–57). Inspection of liver sections from WT and Ptc mice 1 week after BDL (Figure 10, A–D) confirmed our previous report that Ptc mice exhibited an excessive fibroductular response to biliary injury (38). Ptc mice also demonstrated significantly greater induction of various mesenchymal markers, including several matrix genes, such as vimentin (Figure 10E), collagen 1α(I) (Figure 10F), and fibronectin (38). Interestingly, although mRNA levels of *Tgfb1*, a key mediator of both liver cell EMT (14) and liver fibrogenesis (2, 3), were similar after BDL in WT and Ptc mice (Figure 10G), Ptc mice expressed higher levels of the pro-EMT factor *Hmga2* (Figure 10H) and lower levels of *Bmp7*, an EMT inhibitor (Figure 10I), than WT mice after BDL. Thus, the findings in intact mice support the cell culture data displayed in Figures 8 and 9 and together prove that Hh pathway activation plays a key role in inducing liver epithelial cells to undergo EMT and increasing fibrogenesis during cholestatic liver damage.

Discussion

Evidence supporting a role for EMT in repair of chronic liver injury is growing (14–16, 58). The current study demonstrates that activation of the Hh pathway promotes EMT in cholangiocytes. The Hh-regulated transcription factor Gli2 was demonstrated in nuclei of ductular cells that coexpressed epithelial and mesenchymal markers in the livers of humans with chronic biliary fibrosis. Hh pathway activity and markers of EMT also increased in the livers of rats when biliary fibrosis was induced by BDL. Primary cholangiocytes isolated from such rats exhibited both Hh pathway activation (as evidenced by downregulation of the Hh inhibitor *Hhip* and upregulation of Ptc and *Gli2*, Hh target genes),

and gene expression changes typical of cells undergoing EMT. Moreover, when placed in Transwell cocultures with Hh-producing MF-HSCs or treated with conditioned medium from these cells, immature cholangiocytes acquired a migratory phenotype and increased expression of various mesenchymal markers, as well as several factors that promote EMT, while concomitantly repressing expression of epithelial markers and EMT inhibitors. These effects were abrogated by adding Hh-neutralizing antibodies to the MF-HSC–conditioned medium, demonstrating that paracrine Hh signaling induces EMT in cultured cholangiocytes. A similar process likely regulates EMT in vivo, as gene expression changes of EMT and liver fibrogenesis were amplified after BDL in Ptc mice that have an impaired ability to turn off Hh signaling following biliary injury (54–57). Together, these findings support the concept that EMT contributes to the pathogenesis of biliary fibrosis and identify the Hh pathway as an important mediator of this response.

Our results in liver cells are consistent with the acknowledged actions of Hh signaling in other systems. For example, the Hh pathway is known to regulate EMT during fetal development, and this process is required for migration of Hh-responsive cells during tissue morphogenesis (48). Cell migration is also a key feature of cancer invasion and metastasis, and Hh signaling has been shown to play a pivotal role in cancer cell EMT (29, 59, 60). Hh pathway activation has also been shown to be necessary for invasion/migration of nonmalignant cells in adults. For example, progesterone-mediated induction of Hh ligand production by uterine stromal cells is required for embryo implantation (61, 62). Hh signaling also controls the migration of basal epidermal cells to more superficial aspects of adult skin (63, 64). Thus, the new evidence for Hh-mediated induction of EMT in some bile duct epithelial cells during chronic biliary injury suggests that migration of these cells might be involved in remodeling of adult livers with cholestatic damage.

The proximal branches of the intrahepatic biliary tree house the progenitor compartment in adult livers (42), and mobilization of cells from this compartment occurs during the regeneration of chronically injured livers (65). Liver epithelial progenitors are heterogeneous (66). This is thought to reflect their derivation from more primitive, bipotent progenitors that are capable of differentiating along either the hepatocytic or biliary lineages (42, 65, 67). Some of the bipotent progenitors have been shown to exhibit fibroblast-like features that are stabilized by treatment with the profibrogenic cytokine TGF-β. The immediate progeny of these bipotent progenitors also exhibit considerable plasticity, as TGF-β treatment of such immature hepatocytic cells in culture causes them to revert to the fibroblastic phenotype (i.e., undergo EMT). Other manipulations induce mesenchymal-epithelial transitions (MET), by which the fibroblastic cells differentiate into bile ductular or hepatocytic cells (68). Assuming that immature liver cells behave similarly when
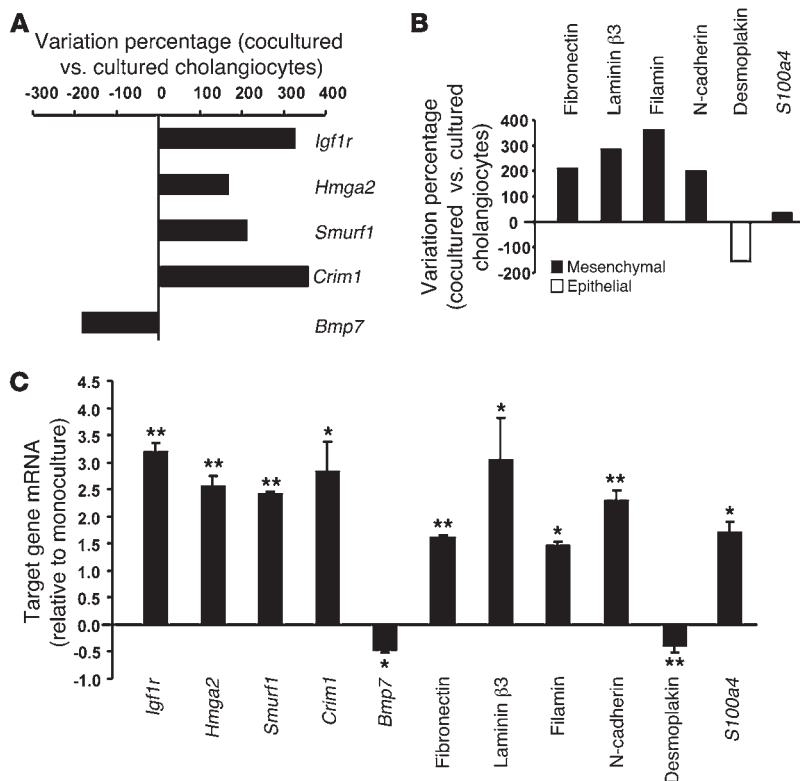
Figure 6

EMT gene profile is induced in cholangiocytes by coculture with myofibroblasts. (**A** and **B**) Microarray probe analysis. The probe expression values of available Affymetrix GeneChips were calculated by means of the Robust Multichip Average (RMA) algorithm, based on the Affymetrix CEL and CDF files as standard inputs. Gene probes having an expression ratio above 1.500 (upper threshold) and below 0.666 (i.e., the reciprocal of 1.500; lower threshold) were considered for analysis. (**A**) Upregulation of *Igf1r*, an EMT signal transducer; *Hmga2*, an EMT transcriptional regulator; SMAD-specific E3 ubiquitin protein ligase 1 (*Smurf1*, a TGF-β signaling effector); and cysteine-rich transmembrane BMP regulator 1 (*Crim1*), with significant downregulation of *Bmp7*, an EMT antagonist. (**B**) Probe analysis revealed the acquisition of mesenchymal phenotype in cocultured cholangiocytes, with loss of epithelial markers (white bars) such as desmoplakin and upregulation of mesenchymal markers (black bars) such as laminin β3, fibronectin, filamin, N-cadherin, and *S100a4*. Complete probe analysis is provided in Supplemental Table 1. (**C**) Microarray data validation by QRT-PCR analysis. Target gene mRNA levels in cocultured cholangiocytes are displayed as fold change relative to monocultures. Data are representative of 3 independent experiments and shown as mean ± SEM. *$P < 0.05$, **$P < 0.005$ versus monoculture.

confronted with TGF-β during fibrosing liver injury, one would predict that EMT occurs in certain types of liver cells when the liver microenvironment becomes enriched with TGF-β and subsides as TGF-β levels decline. Our data in the BDL/R-Y rat model of reversible cholestatic liver damage support this concept.

In non-liver cells, the mechanisms by which TGF-β induces EMT are being delineated, and emerging evidence demonstrates crosstalk with the Hh signaling pathway at several levels. TGF-β1 induces EMT by initiating ALK5-dependent events that lead to activation of Smad-3 and eventual repression of E-cadherin by factors such as Snail and Twist (22). Recently, Hh ligand-receptor interactions that result in Smo activation were shown to enhance this process in gastric cancer cells (25). Smo activation results in nuclear localization of Gli family transcription factors that are known to induce expression of both Snail and Twist (22). Hence, when TGF-β is present, canonical Hh pathway activation stimulates expression of factors that promote EMT by downregulating the epithelial adhesion molecule E-cadherin (69, 70). Recently, we reported that TGF-β1 treatment induces expression of Hh ligands in liver cells (71), identifying a mechanism that helps to explain why both factors accumulate during liver fibrosis. TGF-β has also been shown to induce EMT via noncanonical (i.e., Hh ligand–independent) activation of Gli transcription factors (72).

Our immunohistochemical analyses of liver samples from humans and rats with fibrosing cholestatic liver damage localize EMT to ductular cells with nuclear expression of Gli2, providing the first in vivo evidence to our knowledge that EMT in non-neoplastic adult liver cells is likely to proceed via mechanisms that drive this process in other cell types. During the onset and relief of biliary obstruction in our rat model, expression of collagen gene expression (37) and EMT markers paralleled variations in Hh

ligand expression. Moreover, RNA analysis of primary cholangiocytes from BDL rats demonstrated that these cells strongly downregulate *Hhip*, an Hh ligand antagonist, when undergoing EMT. Therefore, in aggregate, our findings support a role for canonical (i.e., Hh ligand/receptor-initiated) Hh signaling in biliary EMT. This concept is further supported by the evidence for increased EMT following BDL in mice with haploinsufficiency of the Smo inhibitor Ptc, as well as data indicating that treatment with Hh-neutralizing antibodies prevented induction of EMT genes in cultured cholangiocytes. The demonstration that Hh signaling modulates EMT in bile ductular cells opens novel areas for research and has important diagnostic and therapeutic implications for patients with various types of chronic cholestatic liver disease.

Methods

Human subjects

Anonymized liver sections from 5 patients with PBC and 3 control healthy livers were examined. Tissues were obtained from the Università Politecnica delle Marche School of Medicine and the Duke University School of Medicine Tissue Bank Shared Resource and studied under a protocol approved by the Institutional Review Board of Università Politecnica delle Marche and by the Duke University Health System Institutional Review Board, in accordance with NIH guidelines for human subject research.

Immunohistochemistry

Specimens fixed in formalin and embedded in paraffin were cut into 4-μm sections, dewaxed, hydrated, and subsequently incubated for 10 minutes in 3% hydrogen peroxide to block endogenous peroxidase. Antigen retrieval was performed by heating in 10 mM sodium citrate buffer (pH 6.0) for 10 minutes. Sections were blocked in Dako protein
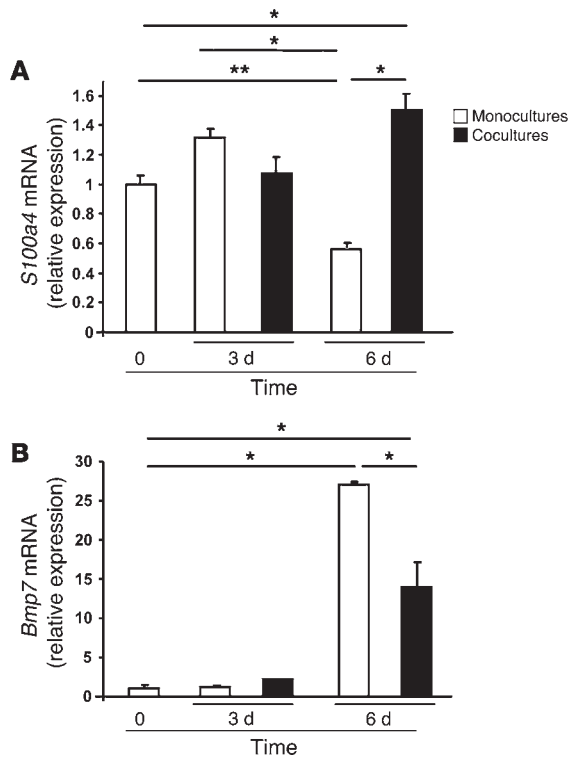
Figure 7

Coculture with MF-HSCs reverses cholangiocytes' tendency to retain epithelial gene expression. Cholangiocytes were cultured alone (monoculture, white bars) or with MF-HSCs (coculture, black bars) and harvested after 3 or 6 days. QRT-PCR analysis was done to assess expression of *S100a4* (**A**) and *Bmp7* (**B**). Results were compared with expression of these genes in freshly plated cholangiocytes (time 0). Data are mean ± SEM of 3 experiments. *$P < 0.05$ and **$P < 0.005$.

tion procedure. For double immunofluorescence staining, cytospin slides with primary cholangiocytes from 1-week sham-operated or BDL rats were used. Samples were fixed and permeabilized, saturated, and processed for immunostaining with primary antibody against S100A4 (A5114; Dako) and Ptc (sc-6149; 1:80; Santa Cruz Biotechnology Inc.). Alexa Fluor 568 and Alexa Fluor 488 (Molecular Probes, Invitrogen) were used as secondary antibodies. DAPI counterstaining was employed to indicate nuclei.

Animals and experimental design

Male Sprague-Dawley rats (Charles River Laboratories) underwent BDL and scission ($n = 18$) as previously described (37) or sham surgery ($n = 4$). Four weeks later, an R-Y was constructed (37, 44, 45) to relieve biliary obstruction, and recovery was monitored over the ensuing 12 weeks. Liver samples were collected at 4 weeks after BDL ($n = 8$) and then at 1 week ($n = 5$) and 12 weeks ($n = 5$) after R-Y. Tissue samples were processed for RNA analysis, and results were compared with those for sham-operated rats. Rat experiments were approved by the government of Lower Franconia, Germany, and the Institutional Review Board of Beth Israel Deaconess Medical Center.

Ptc mice and their WT littermates were obtained from P.A. Beachy (Johns Hopkins University, Baltimore, Maryland, USA) (54). At 8 weeks of age, these mice were subjected to BDL ($n = 6$ per group) and sacrificed after 1 week after surgery (38). Animal studies in mice were approved by the Duke University Medical Center Institutional Animal Care and Use Committee in accordance with the *Guide for the care and use of laboratory animals* (NIH publication no. 85-23. Revised 1985).

block (X9090) for 30 minutes and incubated with primary anti-S100A4 (M7018; 1:2,500; Dako), anti–CK-7 (M7018, 1:750; Dako), anti-vimentin (M7020,1:500; Dako), and anti-Gli2 (ab 26056, 1:1,000; Abcam Ltd). Control sections were incubated overnight at 4°C in each corresponding serum for primary antibody sources. Polymer-HRP anti-rabbit (K4003; Dako) or MACH3 mouse AP polymer kit (MP530; Biocare Medical) were used as secondary antibody. DAB reagent (Dako) and Ferangi Blue Chromogen Kit (FB812S; Biocare Medical) were employed in the detec-

Figure 8

Myofibroblast-derived soluble factors increase motility/migration in cocultured cholangiocytes. (**A**–**F**) Cell migration was assessed by wound-healing assay. Cholangiocytes were cultured in the absence (**A** and **B**) or presence (**C**–**F**) of Transwell filter inserts containing MF-HSCs for 6 days; cholangiocyte monolayers were then scratched, and an image was acquired immediately (time 0; **A**, **C**, and **E**) and 18 hours later after treatment with control IgG (**B**, **D**, and black bars) or Hh-neutralizing antibody (NAb) (**F** and gray bars). Cholangiocyte migration was quantified by measuring the distance dividing the 2 sides of the monolayer using Image J software (**G**) and by counting the numbers of cells that had migrated into the wound after 18 hours (**H**). **$P < 0.005$ versus monocultures, time 0 (**G**) or IgG-treated monoculture (**H**); #$P < 0.005$ versus IgG-treated coculture. Original magnification, ×10 (**A**–**F**). The dashed lines (**A**–**F**) indicate the leading edge of the cut that was made across the monolayers.
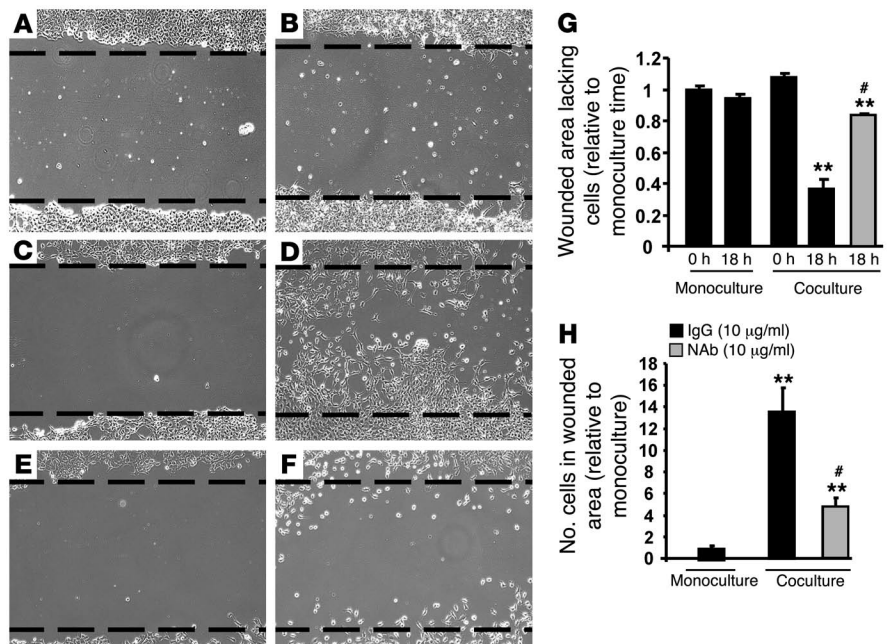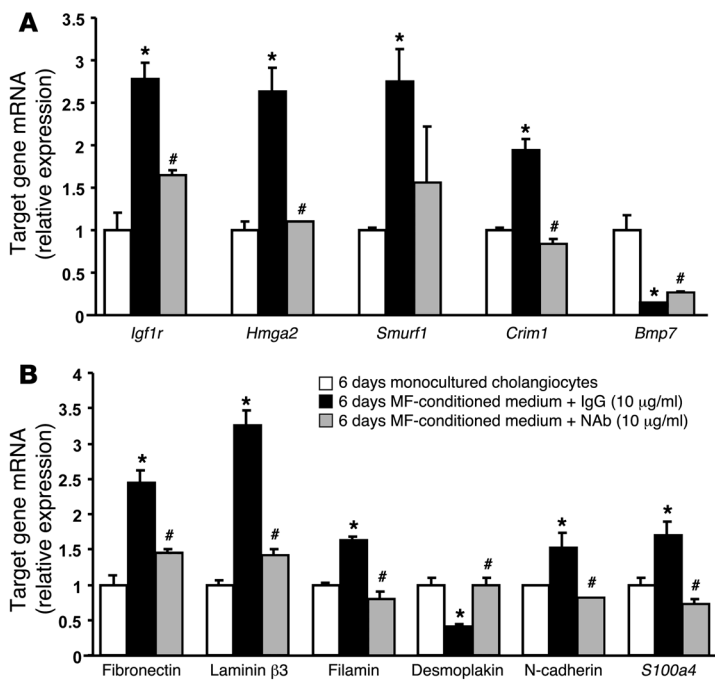
Figure 9
Neutralization of myofibroblast-derived Hh ligands inhibits EMT gene expression profile in cocultured cholangiocytes. Cells of the MF-HSC 8B line were cultured alone for 6 days and conditioned medium was collected. After 18 hours of serum starvation, monocultures of cholangiocyte cell line 603B were treated for an additional 24 hours with MF-HSC–conditioned medium (MF-conditioned medium) in the presence of control IgG (10 μg/ml; black bars) or Hh-neutralizing antibody (10 μg/ml; gray bars). Control cholangiocyte monocultures received regular (not MF-HSC–conditioned) medium (white bars). QRT-PCR was then performed to analyze the expression of EMT-related genes (**A**) and cell markers (**B**) that had been altered by cocultures with MF-HSCs. Results are expressed relative to the control cholangiocytes that received unconditioned medium. Data are representative of 3 independent experiments and expressed as mean ± SEM. *$P < 0.05$ versus control cholangiocytes; #$P < 0.05$ versus cholangiocytes treated with MF-HSC–conditioned medium plus IgG.

Cell isolation and culture

Primary cholangiocytes. Pure cholangiocytes were isolated from 1-week sham-operated or BDL rats as previously described (73, 74). Namely, a monoclonal antibody (IgM; provided by R. Faris, Brown University, Providence, Rhode Island, USA) against an unidentified membrane antigen expressed by all intrahepatic cholangiocytes (73) was used for purification, and purity of cholangiocytes was confirmed by cytochemistry for γGT (74), a specific marker for cholangiocytes (75). At the end of the purification procedure, cell viability was assessed by trypan blue exclusion and was found to be greater than 97%. The isolation protocol was performed by the Scott & White and Texas A&M Health Science Center Institutional Animal Care and Use Committee.

Cell lines and coculture system. Murine cholangiocyte 603B line (76) was kindly provided by Yoshiyuki Ueno (Tohoku University, Sendai, Japan) and G. Gores (Mayo Clinic, Rochester, Minnesota, USA) and maintained in 10% serum-supplemented DMEM (Sigma-Aldrich), 100 U/ml penicillin, and 100 μg/ml streptomycin (GIBCO/BRL, Invitrogen) (38, 77).

Clonally derived rat HSC line (HSC 8B) was obtained from M. Rojkind (George Washington University, Washington D.C., USA) (78) and cultured in 10% serum-supplemented RPMI-1640 medium (GIBCO/BRL, Invitrogen), 10 mM HEPES, 100 IU/ml penicillin, and 100 μg/ml streptomycin (GIBCO/BRL, Invitrogen) (79).

To characterize the effects of mesenchymal-epithelial interactions in vitro, we developed a coculture system in which MF-HSCs and cholangiocyte lines were cultured for 3 and 6 days alone or in a Transwell insert coculture system, using 0.4-μm pore size polyester (PET) inserts (Corning) as previously described (38).

Cell migration. Murine cholangiocyte 603B line was cultured for 6 days in the mono/coculture system described above. A standard wound-healing assay was then performed as previously reported (80). Namely, a wound was manually created by scraping the cell monolayer with P200 pipette tip. Cells were washed twice with PBS and then incubated for additional 18 hours in the original culture/coculture system in the presence of 10 μg/ml Hh-neutralizing antibody (5E1; Developmental Studies Hybridoma Bank) or 10 μg/ml irrelevant IgG (R&D Systems). A reference mark

was created on the dish and a time 0 image was acquired. After 18 hours, a second image was taken in the matched region, and the distance of the wound-healing area lacking cells was quantified with ImageJ software (http://rsbweb.nih.gov/ij/) (80). Additional quantification of cholangiocyte migration was performed by counting the cells that had crossed into wounded area (80).

Hh ligand neutralization in vitro. To evaluate the effect of myofibroblast-derived Hh ligands on cholangiocyte EMT, conditioned medium was collected from 6-day MF-HSC monocultures. Cholangiocytes were serum starved for 18 hours and then treated for 24 hours with MF-HSC–conditioned medium in the presence of Hh-neutralizing antibody or control IgG (10 μg/ml) (38, 81). Total mRNA was extracted, and QRT-PCR for EMT-related genes was performed as described previously (38, 51).

Microarray analysis

RNA isolation and labeling. Total RNA was extracted from cholangiocyte cell line 603B after 6 days of mono- or coculture using TRIzol (Invitrogen), combined with RNeasy columns (QIAGEN) and followed by RNase-free DNase I treatment (QIAGEN) (38, 51). Namely, for each sample (*n* = 3 per group), cholangiocyte total mRNA was harvested and pooled from 6 wells/plate (Corning). Quality control of RNA was assessed using Agilent 2100 Bioanalyzer (Agilent Technologies), and samples were then hybridized to Mouse 430-2 Affymetrix GeneChips (Duke University Microarray Facility).

Data analysis and statistics. The probe expression values of Affymetrix Mouse Genome 430 2.0 GeneChips were calculated applying the Robust Multichip Average (RMA) algorithm by means of RMAExpress (82–84) based on the Affymetrix CEL and CDF files as standard inputs.

Gene probes having an expression ratio (cocultured/monocultured cholangiocytes) above 1.500 (upper threshold) and below 0.666 (i.e., the reciprocal of 1.500; lower threshold), respectively, were considered for the GO analysis (85). Each gene probe was then assigned to its corresponding GO families. Subsequently, GO sets were ranked based on the total number of genes belonging to them (i.e., depending on the GO family size), so that only GO sets having a gene count of at least 2 were used. Additionally, the EASE scores of all GO families were calculated, and GO sets whose
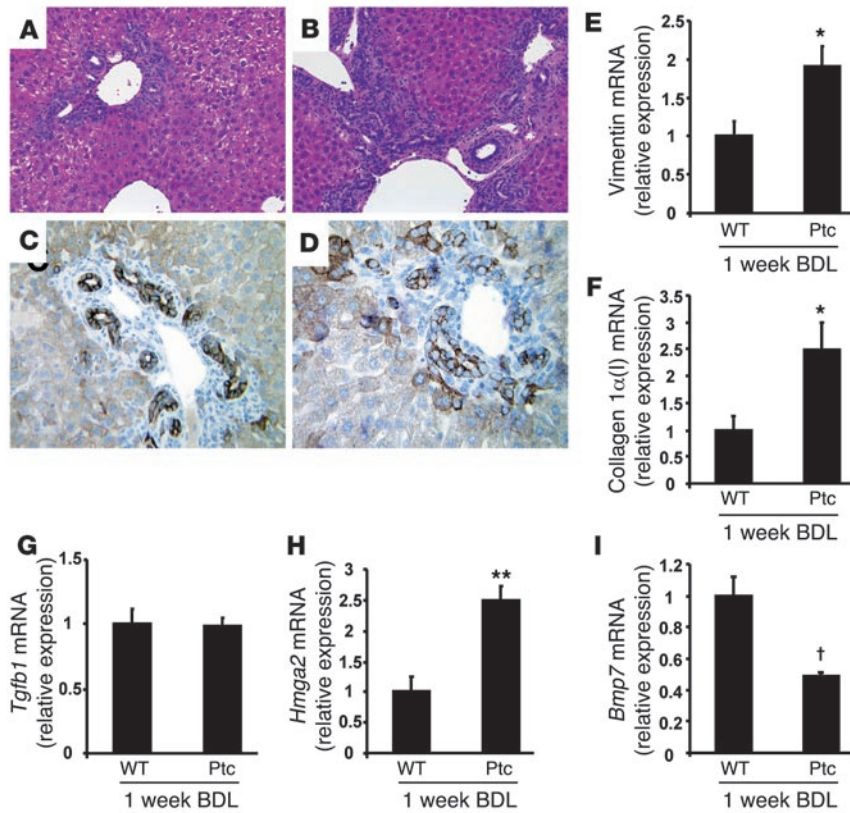
Figure 10
Ptc mice with increased Hh activity exhibit increased EMT after BDL. Liver sections stained with H&E (**A** and **B**) or anti-CK (**C** and **D**) in representative WT mice (**A** and **C**) and Ptc mice (**B** and **D**) after 1-week BDL. QRT-PCR of whole liver tissue from Ptc mice ($n = 6$) and their WT littermates ($n = 6$) after 1 week of BDL. (**E**) Vimentin; (**F**) collagen 1α(I); (**G**) *Tgfb1*; (**H**) *Hmga2*; (**I**) *Bmp7*. Data are shown as mean ± SEM. *$P < 0.05$ versus WT-BDL; **$P < 0.005$, †$P = 0.08$ versus WT-BDL. Original magnification: ×20 (**A** and **B**), ×40 (**C** and **D**).

score was 0.100 or greater were discarded (86, 87). Later, GO families associated with more than 10% of selected genes were also removed, in order to increase the specificity of the GO analysis. The remaining subpopulation of GO sets was ranked based on the family size and, secondarily, on the family EASE score. After assessing the sum of the sizes of all GO families left in the analysis (i.e., total size sum), this pool of GO sets was further split into 2 groups, one whose size sum accounted for at least 60% of total size sum (top group) and the other one accounting for the residual percentage (i.e., for less than 40% of total size sum) (bottom group). In this splitting process, when 2 or more GO families had the same size they were assigned to the same group (top or bottom). Finally, a pie chart was generated using individual names for the top group of GO families, while GO sets belonging to the bottom group were collectively designated as "other."

Microarray validation by QRT-PCR. After DNase I treatment (QIAGEN), 1 μg of RNA was reverse transcribed to cDNA templates using random primers and SuperScript RNase H⁻ Reverse Transcriptase (Invitrogen) and amplified. Semiquantitative QRT-PCR was performed as described below.

Two-step real-time RT-PCR
Total RNA was extracted from cholangiocyte cell line, primary cholangiocytes, or 300–400 mg of homogenized liver pieces from median and right lobes using a combination of TRIzol (Invitrogen) and RNeasy columns (QIAGEN) (38, 51). After RNase-free DNase I treatment (QIAGEN), 1 μg of RNA was reverse transcribed to cDNA templates using random primers and SuperScript RNase H⁻ Reverse Transcriptase and amplified. For semiquantitative QRT-PCR, 1.5% of the first-strand reaction was amplified using iQ-SYBR Green Supermix (Bio-Rad), an iCycler iQ Real-Time Detection System, and specific primers for target sequences, as well as 18S (38).

The sequences of primers for mouse were as follows: *Igf1r* forward, 5′-CCAAAGTCTGCGGCGATGAA-3′, reverse, 5′-TAGCCGGTCAC-

CACCTCGAT-3′; *Hmga2* forward, 5′-GGTGCCACAGAAGCGAGGAC-3′, reverse, 5′-CTGCGGACTCTTGCGAGGAT-3′; *Crim1* forward, 5′-CCG-GCTGCAACATAATCAA-3′, reverse, 5′-AGCATAGCCCTCGATCAGAA-3′; *Smurf1* forward, 5′-AGTTCCAGAGGCGTCCATC-3′, reverse, 5′-CGCT-GCAATTCCCTTACCTA-3′; *Bmp7* forward, 5′-GTGGTCAACCCTCG-GCACA-3′, reverse, 5′-GGCGTCTTGGAGCGATTCTG-3′; fibronectin forward, 5′-GTGGCTGCCTTCAACTTCTC-3′, reverse, 5′-GTGGGTTG-CAAACCTTCAAT-3′; filamin forward, 5′-TAAGTATGCCGTTCGCT-TCA-3′, reverse, 5′-CAAGCCCAGCACCGTAG-3′; laminin β3 forward, 5′-CCTGGCTTCTCGGTTGCTA-3′, reverse, 5′-GGTACATAAGGAG-GAGCCGACT-3′; N-cadherin forward, 5′-CAGTGGACATCAATGGCAAT-CA-3′, reverse, 5′-CATTTGGATCATCCGCATCA-3′; desmoplakin forward, 5′-GCTGCACCGTCAACGACCA-3′, reverse, 5′-GCTGCATCCCTTCTCC-GAATTT-3′; vimentin forward, 5′-GCTTCTCTGGCACGTCTTGA-3′, reverse, 5′-CGCAGGGCATCGTTGTTC-3′; collagen1α(I) forward, 5′-GAGC-GGAGAGTACTGGATCG-3′, reverse, 5′-GCTTCTTTTCCTTGGGGTTC-3′; *S100a4* forward, 5′-AAAGAGGGTGACAAGTTCAA-3′, reverse, 5′-CGG-GGTTCCTTATCTGG-3′; *18S* forward, 5′-TTGACGGAAGGGCACCAC-CAG-3′, reverse, 5′-GCACCACCACCCACGGAATCG-3′.

The sequences of primers for rat were as follows: *S100a4* forward, 5′-ATACTCAGGCAACGAGGGTG-3′, reverse, 5′-CTTCCGGGGCTCCT-TATC-3′; *Aqp1* forward, 5′-TGTGCCGTGGATCGAC-3′, reverse, 5′-CAA-CATGGCCAGCGAAAT-3′; *CK19* forward, 5′-GTCCACACTACGCA-GATCCA-3′, reverse, 5′-CAAGCAGGCTTCGGTAGGT-3′; *CK7* forward, 5′-TAGAGTCCAGCATCGCAGAG-3′, reverse, 5′-CACAGGTCCCATTCC-GTC-3′; *Gli2* forward, 5′-ATAAGCGGAGCAAGGTCAAG-3′, reverse, 5′-CAGTGGCAGTTGGTCTCGTA-3′; *Hhip* forward, 5′-TGTGCCGTG-GATCGAC-3′, reverse, 5′-GATCTCCGAACACGTAGCTT-3′; *18S* forward, 5′-TTGACGGAAGGGCACCACCAG-3′, reverse, 5′-GCACCACCACC-CACGGAATCG-3′.

For all primer pairs, specificity was confirmed by cloning and sequencing of PCR products, and optimal annealing temperature and melt curve were determined. Threshold cycles (C_t) were automatically calculated by the iCycler iQ Real-Time Detection System. Target gene levels in treated cells or tissues are presented as a ratio to levels detected in corresponding control cells or tissues, according to the $\Delta\Delta C_t$ method (37, 38).

Statistical analysis

Results are expressed as mean ± SEM, unless indicated otherwise. Comparisons between groups were performed using the 2-tailed Student's t test. Significance was accepted when P was less than 0.05.

1. Lazaridis, K.N., Strazzabosco, M., and Larusso, N.F. 2004. The cholangiopathies: disorders of biliary epithelia. *Gastroenterology*. **127**:1565–1577.
2. Kisseleva, T., and Brenner, D.A. 2008. Mechanisms of fibrogenesis. *Exp. Biol. Med. (Maywood)*. **233**:109–122.
3. Bataller, R., and Brenner, D.A. 2005. Liver fibrosis. *J. Clin. Invest.* **115**:209–218.
4. Milani, S., et al. 1990. Procollagen expression by nonparenchymal rat liver cells in experimental biliary fibrosis. *Gastroenterology*. **98**:175–184.
5. Kinnman, N., et al. 2003. The myofibroblastic conversion of peribiliary fibrogenic cells distinct from hepatic stellate cells is stimulated by platelet-derived growth factor during liver fibrogenesis. *Lab. Invest.* **83**:163–173.
6. Kinnman, N., et al. 2000. PDGF-mediated chemoattraction of hepatic stellate cells by bile duct segments in cholestatic liver injury. *Lab. Invest.* **80**:697–707.
7. Kinnman, N., et al. 2001. Hepatic stellate cell proliferation is an early platelet-derived growth factor-mediated cellular event in rat cholestatic liver injury. *Lab. Invest.* **81**:1709–1716.
8. Friedman, S.L., Roll, F.J., Boyles, J., and Bissell, D.M. 1985. Hepatic lipocytes: the principal collagen-producing cells of normal rat liver. *Proc. Natl. Acad. Sci. U. S. A.* **82**:8681–8685.
9. Tuchweber, B., et al. 1996. Proliferation and phenotypic modulation of portal fibroblasts in the early stages of cholestatic fibrosis in the rat. *Lab. Invest.* **74**:265–278.
10. Li, Z., et al. 2007. Transforming growth factor-beta and substrate stiffness regulate portal fibroblast activation in culture. *Hepatology*. **46**:1246–1256.
11. Kruglov, E.A., Nathanson, R.A., Nguyen, T., and Dranoff, J.A. 2006. Secretion of MCP-1/CCL2 by bile duct epithelia induces myofibroblastic transdifferentiation of portal fibroblasts. *Am. J. Physiol. Gastrointest. Liver Physiol.* **290**:G765–G771.
12. Jhandier, M.N., Kruglov, E.A., Lavoie, E.G., Sevigny, J., and Dranoff, J.A. 2005. Portal fibroblasts regulate the proliferation of bile duct epithelia via expression of NTPDase2. *J. Biol. Chem.* **280**:22986–22992.
13. Kisseleva, T., et al. 2006. Bone marrow-derived fibrocytes participate in pathogenesis of liver fibrosis. *J. Hepatol.* **45**:429–438.
14. Rygiel, K.A., et al. 2008. Epithelial-mesenchymal transition contributes to portal tract fibrogenesis during human chronic liver disease. *Lab. Invest.* **88**:112–123.
15. Robertson, H., Kirby, J.A., Yip, W.W., Jones, D.E., and Burt, A.D. 2007. Biliary epithelial-mesenchymal transition in posttransplantation recurrence of primary biliary cirrhosis. *Hepatology*. **45**:977–981.
16. Kalluri, R., and Neilson, E.G. 2003. Epithelial-mesenchymal transition and its implications for fibrosis. *J. Clin. Invest.* **112**:1776–1784.
17. Iwano, M., et al. 2002. Evidence that fibroblasts derive from epithelium during tissue fibrosis. *J. Clin. Invest.* **110**:341–350.
18. Thiery, J.P. 2003. Epithelial-mesenchymal transitions in development and pathologies. *Curr. Opin. Cell Biol.* **15**:740–746.
19. Guarino, M., Micheli, P., Pallotti, F., and Giordano, F. 1999. Pathological relevance of epithelial and mesenchymal phenotype plasticity. *Pathol. Res. Pract.* **195**:379–389.
20. Lee, J.M., Dedhar, S., Kalluri, R., and Thompson, E.W. 2006. The epithelial-mesenchymal transition: new insights in signaling, development, and disease. *J. Cell Biol.* **172**:973–981.
21. Xue, C., Plieth, D., Venkov, C., Xu, C., and Neilson, E.G. 2003. The gatekeeper effect of epithelial-mesenchymal transition regulates the frequency of breast cancer metastasis. *Cancer Res.* **63**:3386–3394.
22. Huber, M.A., Kraut, N., and Beug, H. 2005. Molecular requirements for epithelial-mesenchymal transition during tumor progression. *Curr. Opin. Cell Biol.* **17**:548–558.
23. Huber, M.A., et al. 2004. NF-kappaB is essential for epithelial-mesenchymal transition and metastasis in a model of breast cancer progression. *J. Clin. Invest.* **114**:569–581.
24. Zhou, B.P., and Hung, M.C. 2005. Wnt, hedgehog and snail: sister pathways that control by GSK-3beta and beta-Trcp in the regulation of metastasis. *Cell Cycle*. **4**:772–776.
25. Yoo, Y.A., Kang, M.H., Kim, J.S., and Oh, S.C. 2008. Sonic hedgehog signaling promotes motility and invasiveness of gastric cancer cells through TGF-beta-mediated activation of the ALK5-Smad 3 pathway. *Carcinogenesis*. **29**:480–490.
26. Thayer, S.P., et al. 2003. Hedgehog is an early and late mediator of pancreatic cancer tumorigenesis. *Nature*. **425**:851–856.
27. Pasca di Magliano, M., and Hebrok, M. 2003. Hedgehog signalling in cancer formation and maintenance. *Nat. Rev. Cancer*. **3**:903–911.
28. Karhadkar, S.S., et al. 2004. Hedgehog signalling in prostate regeneration, neoplasia and metastasis. *Nature*. **431**:707–712.
29. Bailey, J.M., Singh, P.K., and Hollingsworth, M.A. 2007. Cancer metastasis facilitated by developmental pathways: Sonic hedgehog, Notch, and bone morphogenic proteins. *J. Cell. Biochem.* **102**:829–839.
30. Sicklick, J.K., et al. 2006. Hedgehog signaling maintains resident hepatic progenitors throughout life. *Am. J. Physiol. Gastrointest. Liver Physiol.* **290**:G859–G870.
31. Omenetti, A., and Diehl, A.M. 2008. The adventures of Sonic hedgehog in development and repair. II. Sonic hedgehog and liver development, inflammation, and cancer. *Am. J. Physiol. Gastrointest. Liver Physiol.* **294**:G595–G598.
32. Beachy, P.A., Karhadkar, S.S., and Berman, D.M. 2004. Tissue repair and stem cell renewal in carcinogenesis. *Nature*. **432**:324–331.
33. Watkins, D.N., et al. 2003. Hedgehog signalling within airway epithelial progenitors and in small-cell lung cancer. *Nature*. **422**:313–317.
34. Kalderon, D. 2000. Transducing the hedgehog signal. *Cell*. **103**:371–374.
35. Chuang, P.T., and McMahon, A.P. 1999. Vertebrate Hedgehog signalling modulated by induction of a Hedgehog-binding protein. *Nature*. **397**:617–621.
36. Chuang, P.T., Kawcak, T., and McMahon, A.P. 2003. Feedback control of mammalian Hedgehog signaling by the Hedgehog-binding protein, Hip1, modulates Fgf signaling during branching morphogenesis of the lung. *Genes Dev.* **17**:342–347.
37. Omenetti, A., et al. 2008. The hedgehog pathway regulates remodeling responses to biliary obstruction in rats. *Gut*. Online publication ahead of print. doi:10.1136/gut.2008.148619.
38. Omenetti, A., et al. 2007. Hedgehog-mediated mesenchymal-epithelial interactions modulate hepatic response to bile duct ligation. *Lab. Invest.* **87**:499–514.
39. Jung, Y., McCall, S.J., Li, Y.X., and Diehl, A.M. 2007. Bile ductules and stromal cells express hedgehog ligands and/or hedgehog target genes in primary biliary cirrhosis. *Hepatology*. **45**:1091–1096.
40. Strutz, F., et al. 1995. Identification and characterization of a fibroblast marker: FSP1. *J. Cell Biol.* **130**:393–405.
41. Okada, H., Danoff, T.M., Kalluri, R., and Neilson, E.G. 1997. Early role of Fsp1 in epithelial-mesenchymal transformation. *Am. J. Physiol.* **273**:F563–F574.
42. Libbrecht, L., and Roskams, T. 2002. Hepatic progenitor cells in human liver diseases. *Semin. Cell Dev. Biol.* **13**:389–396.
43. van Eyken, P., Sciot, R., van Damme, B., de Wolf-Peeters, C., and Desmet, V.J. 1987. Keratin immunohistochemistry in normal human liver. Cytokeratin pattern of hepatocytes, bile ducts and acinar gradient. *Virchows Arch. A Pathol. Anat. Histopathol.* **412**:63–72.

44. Raetsch, C., et al. 2002. Pentoxifylline downregulates profibrogenic cytokines and procollagen I expression in rat secondary biliary fibrosis. *Gut.* **50**:241–247.

45. Boigk, G., et al. 1997. Silymarin retards collagen accumulation in early and advanced biliary fibrosis secondary to complete bile duct obliteration in rats. *Hepatology.* **26**:643–649.

46. Thiery, J.P., and Sleeman, J.P. 2006. Complex networks orchestrate epithelial-mesenchymal transitions. *Nat. Rev. Mol. Cell Biol.* **7**:131–142.

47. Marinelli, R.A., and LaRusso, N.F. 1997. Aquaporin water channels in liver: their significance in bile formation. *Hepatology.* **26**:1081–1084.

48. Nagase, T., Nagase, M., Machida, M., and Yamagishi, M. 2007. Hedgehog signaling: a biophysical or biomechanical modulator in embryonic development? *Ann. N. Y. Acad. Sci.* **1101**:412–438.

49. Xia, J.L., Dai, C., Michalopoulos, G.K., and Liu, Y. 2006. Hepatocyte growth factor attenuates liver fibrosis induced by bile duct ligation. *Am. J. Pathol.* **168**:1500–1512.

50. Sicklick, J.K., et al. 2005. Role for hedgehog signaling in hepatic stellate cell activation and viability. *Lab. Invest.* **85**:1368–1380.

51. Yang, L., et al. 2008. Sonic hedgehog is an autocrine viability factor for myofibroblastic hepatic stellate cells. *J. Hepatol.* **48**:98–106.

52. Venkov, C.D., et al. 2007. A proximal activator of transcription in epithelial-mesenchymal transition. *J. Clin. Invest.* **117**:482–491.

53. Wilkinson, L., et al. 2003. CRIM1 regulates the rate of processing and delivery of bone morphogenetic proteins to the cell surface. *J. Biol. Chem.* **278**:34181–34188.

54. Goodrich, L.V., Milenkovic, L., Higgins, K.M., and Scott, M.P. 1997. Altered neural cell fates and medulloblastoma in mouse patched mutants. *Science.* **277**:1109–1113.

55. Lee, Y., et al. 2006. Patched2 modulates tumorigenesis in patched1 heterozygous mice. *Cancer Res.* **66**:6964–6971.

56. Uhmann, A., et al. 2005. A model for PTCH1/Ptch1-associated tumors comprising mutational inactivation and gene silencing. *Int. J. Oncol.* **27**:1567–1575.

57. Wetmore, C., Eberhart, D.E., and Curran, T. 2000. The normal patched allele is expressed in medulloblastomas from mice with heterozygous germ-line mutation of patched. *Cancer Res.* **60**:2239–2246.

58. Diaz, R., et al. 2008. Evidence for the epithelial to mesenchymal transition in biliary atresia fibrosis. *Hum. Pathol.* **39**:102–115.

59. Feldmann, G., et al. 2007. Blockade of hedgehog signaling inhibits pancreatic cancer invasion and metastases: a new paradigm for combination therapy in solid cancers. *Cancer Res.* **67**:2187–2196.

60. Kelleher, F.C., Fennelly, D., and Rafferty, M. 2006. Common critical pathways in embryogenesis and cancer. *Acta Oncol.* **45**:375–388.

61. Kurihara, I., et al. 2007. COUP-TFII mediates progesterone regulation of uterine implantation by controlling ER activity. *PLoS Genet.* **3**:e102.

62. Lee, K., et al. 2006. Indian hedgehog is a major mediator of progesterone signaling in the mouse uterus. *Nat. Genet.* **38**:1204–1209.

63. Adolphe, C., et al. 2004. An in vivo comparative study of sonic, desert and Indian hedgehog reveals that hedgehog pathway activity regulates epidermal stem cell homeostasis. *Development.* **131**:5009–5019.

64. Nieuwenhuis, E., et al. 2006. Mice with a targeted mutation of patched2 are viable but develop alopecia and epidermal hyperplasia. *Mol. Cell. Biol.* **26**:6609–6622.

65. Fausto, N. 2004. Liver regeneration and repair: hepatocytes, progenitor cells, and stem cells. *Hepatology.* **39**:1477–1487.

66. Parent, R., Marion, M.J., Furio, L., Trepo, C., and Petit, M.A. 2004. Origin and characterization of a human bipotent liver progenitor cell line. *Gastroenterology.* **126**:1147–1156.

67. Michalopoulos, G.K. 2007. Liver regeneration. *J. Cell. Physiol.* **213**:286–300.

68. Spagnoli, F.M., Cicchini, C., Tripodi, M., and Weiss, M.C. 2000. Inhibition of MMH (Met murine hepatocyte) cell differentiation by TGF(beta) is abrogated by pre-treatment with the heritable differentiation effector FGF1. *J. Cell Sci.* **113**:3639–3647.

69. Li, X., Deng, W., Lobo-Ruppert, S.M., and Ruppert, J.M. 2007. Gli1 acts through Snail and E-cadherin to promote nuclear signaling by beta-catenin. *Oncogene.* **26**:4489–4498.

70. Li, X., et al. 2006. Snail induction is an early response to Gli1 that determines the efficiency of epithelial transformation. *Oncogene.* **25**:609–621.

71. Jung, Y., et al. 2008. Accumulation of hedgehog-responsive progenitors parallels alcoholic liver disease severity in mice and humans. *Gastroenterology.* **134**:1532–1543.

72. Lauth, M., and Toftgard, R. 2007. Non-canonical activation of GLI transcription factors: implications for targeted anti-cancer therapy. *Cell Cycle.* **6**:2458–2463.

73. Ishii, M., Vroman, B., and LaRusso, N.F. 1989. Isolation and morphologic characterization of bile duct epithelial cells from normal rat liver. *Gastroenterology.* **97**:1236–1247.

74. Marzioni, M., et al. 2007. Glucagon-like peptide-1 and its receptor agonist exendin-4 modulate cholangiocyte adaptive response to cholestasis. *Gastroenterology.* **133**:244–255.

75. Alpini, G., Lenzi, R., Sarkozi, L., and Tavoloni, N. 1988. Biliary physiology in rats with bile ductular cell hyperplasia. Evidence for a secretory function of proliferated bile ductules. *J. Clin. Invest.* **81**:569–578.

76. Yahagi, K., et al. 1998. Primary culture of cholangiocytes from normal mouse liver. *In Vitro Cell Dev. Biol. Anim.* **34**:512–514.

77. Ishimura, N., Bronk, S.F., and Gores, G.J. 2005. Inducible nitric oxide synthase up-regulates Notch-1 in mouse cholangiocytes: implications for carcinogenesis. *Gastroenterology.* **128**:1354–1368.

78. Greenwel, P., et al. 1991. Characterization of fat-storing cell lines derived from normal and CCl4-cirrhotic livers. Differences in the production of interleukin-6. *Lab. Invest.* **65**:644–653.

79. Schaefer, B., et al. 2003. Reciprocal modulation of matrix metalloproteinase-13 and type I collagen genes in rat hepatic stellate cells. *Am. J. Pathol.* **162**:1771–1780.

80. Rodriguez, L.G., Wu, X., and Guan, J.L. 2005. Wound-healing assay. *Methods Mol. Biol.* **294**:23–29.

81. Ericson, J., Morton, S., Kawakami, A., Roelink, H., and Jessell, T.M. 1996. Two critical periods of Sonic Hedgehog signaling required for the specification of motor neuron identity. *Cell.* **87**:661–673.

82. Bolstad, B.M., Irizarry, R.A., Astrand, M., and Speed, T.P. 2003. A comparison of normalization methods for high density oligonucleotide array data based on variance and bias. *Bioinformatics.* **19**:185–193.

83. Irizarry, R.A., et al. 2003. Summaries of Affymetrix GeneChip probe level data. *Nucleic Acids Res.* **31**:e15.

84. Irizarry, R.A., et al. 2003. Exploration, normalization, and summaries of high density oligonucleotide array probe level data. *Biostatistics.* **4**:249–264.

85. Gene Ontology Consortium. 2001. Creating the gene ontology resource: design and implementation. *Genome Res.* **11**:1425–1433.

86. Dennis, G., Jr., et al. 2003. DAVID: Database for Annotation, Visualization, and Integrated Discovery. *Genome Biol.* **4**:P3.

87. Hosack, D.A., et al. 2003. Identifying biological themes within lists of genes with EASE. *Genome Biol.* **4**:R70.